VLASS Project Memo #25

Investigation of Minimum UV-Range Cutoff for VLASS Single Epoch Calibration

T.M. Candelaria, A.E. Kimball, J.J. Tobin

January 13, 2026

Abstract

We present a study regarding the use of *uv*-ranges with the VLASS Calibration pipeline. The VLASS Calibration pipeline assumes a point source for complex gain calibration, but not all calibrators exhibit minimal structure at short baselines. We review the problem of resolved calibrators used within the VLASS survey and how calibrators that may require *uv*-ranges are considered in complex gain calibration. For the calibration we use an amplitude versus UV-wave plot to determine where the source is point-like and apply this range to the calibration. From there, we select multiple images (four shown here) to visually inspect the impact. We find that there is little visual impact on the source morphologies in the images. Additionally, we investigate, using source catalogs from images in two tiles, the impact of a *uv*-range in their standard calibration. We do not find scientifically relevant impacts on the source catalogs created from images that use *uv*-range relative to those that did not. Overall, we do not recommend using a *uv*-range for VLASS calibration as they have shown to not be necessary.

1 Introduction

The VLASS Single Epoch Calibration pipeline assumes a point source for complex gain calibration. However, not all calibrators exhibit minimal structure at all baselines. Previously, VLASS Memo #19 discusses the use of calibrator spatial models with the VLASS Calibration pipeline. The VLASS team investigated whether a calibrator needs a model based on a $> \pm 3\%$ variation of baselines shorter than 35 kλ and/or at baselines longer than 90 kλ. They found little visual impact on the source morphologies, nor the source catalog flux densities. They determined that spatial models are not required to meet the science goals of the survey and they do not recommend that the survey perform special processing on the data previously suggested to require a calibrator spatial model. However, the models are for small scale structure that specifically affects the mid and long baseline data.

In this study, we investigate the effects of large scale calibrator structure (short baselines) on complex gain solutions for two calibrators, J1522+3144 and J2121+1901. These calibrators were chosen because of their significant structure seen on short baselines in amplitude versus *uv*-wave plots. Figure 1 shows the *uv*-wave plot for J1522, the complex gain calibrator used for tile T19t20, and the *uv*-wave plot for J2121, the complex gain calibrator used for tile T16t29. Using these amplitude versus *uv*-wave plots, we determine a cutoff for the *uv*-range such that the data used for complex gain calibration are point-like. The minimum *uv*-wave cutoff used for J1522+3144 is 25 kλ and 36 kλ for J2121+1901. Calibrations are reprocessed with the determined *uv*-range and imaged using the standard VLASS pipelines for Single Epoch (SE), which includes self-calibration. We image eight regions for two given tiles, with and without a *uv*-range minimum applied to the calibration, to determine if/how much the image improves with this *uv*-range constraint. Each image consists of a 1×1 square degree image.

2 Comparison of Imaging With and Without UV-range

2.1 Comparison of Images

We first compare images visually by comparing a point source in the image, although not necessarily at the phase center. We then compute division maps (uvrange image divided by non-uvrange image) to inspect morphology of the point source. It is imperative to compare the morphology of the sources in both images to determine if there is any impact from using a *uv*-range during calibration. We compare Single Epoch (SE) images because self-calibration is applied, which could compensate for complex gain calibration errors that result from the resolved calibrator at short baselines. We present examples of point sources for three images

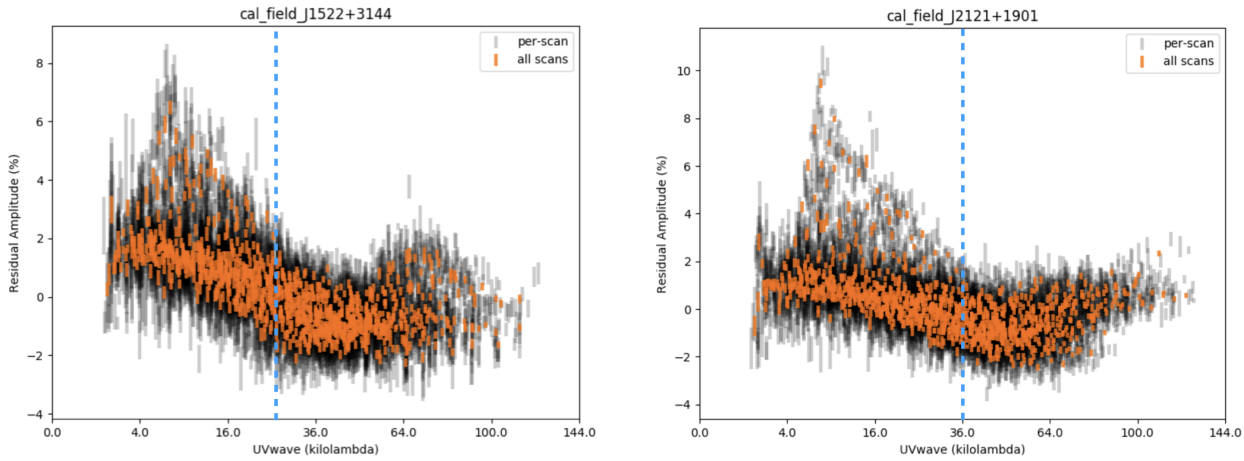

(a) (b)

Figure 1: (a) Plot of the residual amplitudes vs. *uv*-distance for J1522+3144, the complex gain calibrator used for T19t20, in VLASS Epoch 2.1. (b) Plot of the residual amplitudes vs. *uv*-distance for J2121+1901, the complex gain calibrator used for T16t29, in VLASS Epoch 2.2.

chosen in tile T19t20, although a dozen point sources from different images were analyzed overall and present similar findings. We see negligible differences visually for all sources analyzed, including the examples shown below. There is no obvious impact on the emission morphology of the sources that would motivate us to favor the data be calibrated with a *uv*-range over the standard calibration.

2.1.1 T19t20 – J152412+353000

For J152412+353000, total flagging is very similar at 19.57% for the calibration processed with a *uv*-range and 19.87% for the calibration processed without a *uv*-range. Figure 2 displays the chosen point source and region (in red) used for component fitting of the source. Table 1 provides details for this fit for both calibrations as well as the relative differences (in units of sigma) between the parameters fit.

We see minimal differences visually between the images. Quantitatively, we calculate the relative differences (in units of sigma) for each fitting parameter of the point source and find negligible differences. For J152412+353000, the relative differences (in units of sigma) are less than 0.87σ for all parameters. Additionally, Figure 3 shows the region of the source (in red) and the division map for the same region. Division maps (images with *uv*-range applied divided by those without) yield values near unity at point source locations, indicating no significant morphological differences.

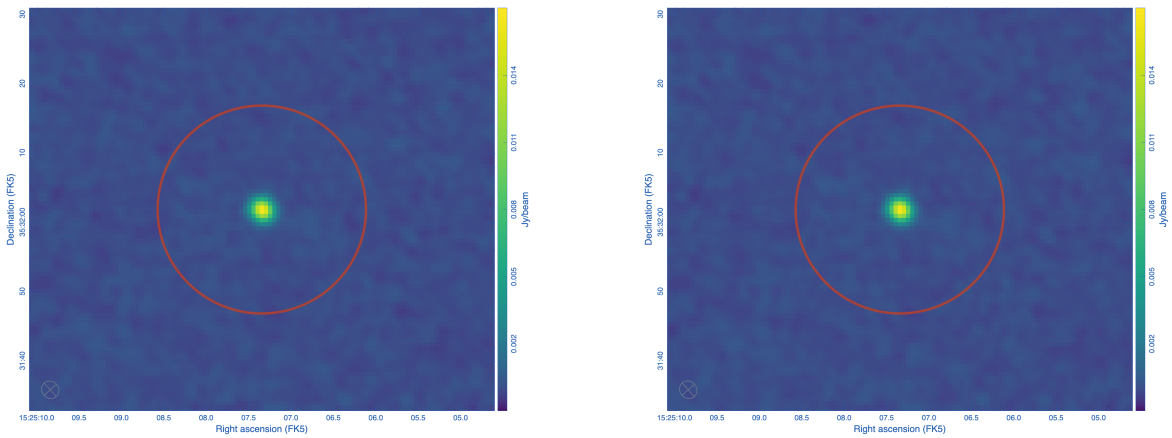

(a) (b)

Figure 2: Point source in J152412+353000 with a *uv*-range applied to the calibration in (a) and without the *uv*-range in (b). The RA and Dec of the point source is 15:25:07.35 35:32:01.9.

	UV-range	**No UV-range**	**Relative Difference**
Center X (arcsec)	15:25:07.34 ± 0.000555	15:25:07.34 ± 0.000552	0.0512
Center Y (arcsec)	35:32:01.87 ± 0.00772	35:32:01.87 ± 0.00786	0.300
Amplitude (Jy/beam)	0.0165 ± 0.000119	0.0167 ± 0.000121	0.833
Major Axis (arcsec)	2.71 ± 0.020	2.72 ± 0.0206	0.246
Minor Axis (arcsec)	2.50 ± 0.0173	2.49 ± 0.0173	0.298
P.A. (deg)	59.73 ± 3.44	53.94 ± 3.20	0.872
Integrated flux (Jy)	0.0177 ± 0.000216	0.0178 ± 0.000219	0.230

Table 1: Comparison of component parameters for a point source in J152412+353000.

2.1.2 T19t20 – J154321+343000

For this image, total flagging is 22.34% for the calibration processed with a *uv*-range and 19.40% for the calibration processed without a *uv*-range. Figure 6 displays the chosen point source and region (in red) used for component fitting of the source. Table 2 provides details for this fit for both calibrations.

We calculate the relative differences (in units of sigma) for each fitting parameter of the point source. For J154321+343000, the relative differences (in units of sigma) are larger for the major and minor axes and the integrated flux than for position and amplitude. Because the errors are quite smaller for the integrated flux, we should expect the relative difference to be larger, similarly for the major and minor axes. Similar to J152412+353000, we see in Figure 5 that the division maps yield values near unity at point source locations, indicating no significant morphological differences.

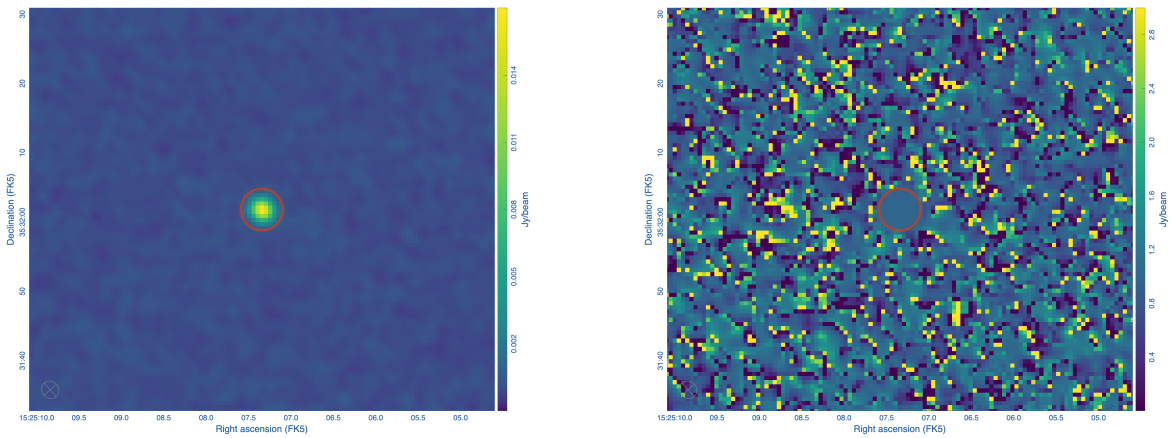

(a) (b)

Figure 3: (a) displays the point source for the image with *uv*-range applied calibration and (b) displays the same region (in red) of the uvrange image divided by the non-uvrange data.

	UV-range	**No UV-range**	**Relative Difference**
Center X (arcsec)	15:43:07.42 ± 0.000198	15:43:07.42± 0.000208	0.390
Center Y (arcsec)	32:43:52.59 ± 0.00307	32:43:52.59 ± 0.00317	0.341
Amplitude (Jy/beam)	0.0426 ± 0.00114	0.0445 ± 0.00122	0.805
Major Axis (arcsec)	2.80 ± 0.00814	2.87 ± 0.0085	4.207
Minor Axis (arcsec)	2.38 ± 0.00588	2.44 ± 0.00615	4.986
P.A. (deg)	41.87 ± 0.611	43.67 ± 0.628	1.453
Integrated flux (Jy)	0.0434 ± 0.000201	0.0454 ± 0.000215	4.808

Table 2: Comparison of component parameters for a point source in J154321+343000.

2.1.3 T19t20 – J155758+353000

For this image, total flagging is 20.73% for the calibration processed with a *uv*-range and 20.43% for the calibration processed without a *uv*-range. Figure 6 displays the chosen point source and region (in red) used to for component fitting of the source. Table 3 provides details for this fit for both calibrations.

Lastly, in Figure 7, we see that the division maps yield values near unity at point source locations, indicating no significant morphological differences.

2.1.4 T16t29 – J211512+233000

For this image, we display the chosen point source and region used for component fitting in Figure 8, and Table 4 provides details for this fit for both calibrations.

We calculate the relative differences (in units of sigma) for each fitting parameter of the point source. For J211512+233000, the relative differences (in units of sigma) are larger for

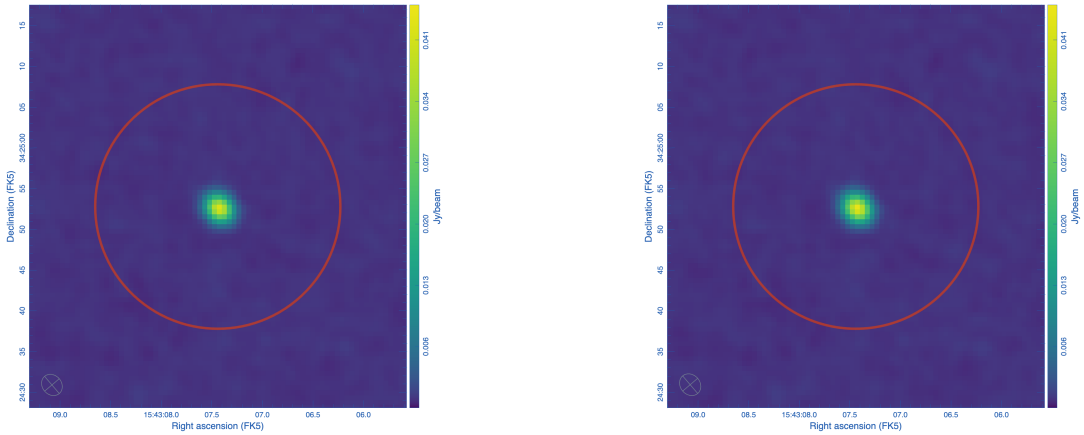

(a) (b)

Figure 4: Point source in J154321+343000 with a *uv*-range applied to the calibration in (a) and without the *uv*-range in (b). The RA and Dec of the point source is 15:43:07.44 34:24:52.8

	UV-range	**No UV-range**	**Relative Difference**
Center X (arcsec)	15:56:29.49 ± 0.000069	15:56:29.49 ± 0.000072	1.762
Center Y (arcsec)	35:44:32.73 ± 0.00123	35:44:32.73 ± 0.00126	0.112
Amplitude (Jy/beam)	0.154 ± 0.00163	0.153 ± 0.00167	0.330
Major Axis (arcsec)	2.63 ± 0.0029	2.65 ± 0.00305	2.54
Minor Axis (arcsec)	2.37 ± 0.0024	2.37 ± 0.02245	1.383
P.A. (deg)	18.12 ± 0.391	22.45 ± 0.384	5.587
Integrated flux (Jy)	0.155 ± 0.000285	0.155 ± 0.000292	1.400

Table 3: Comparison of component parameters for a point source in J155758+353000.

the major and minor axes than for position, amplitude, and integrated intensity. Because the errors are quite smaller for the major and minor axes, we should expect the relative difference to be larger. Similar to J152412+353000, we see in Figure 9 that the division maps yield values near unity at point source locations, indicating no significant morphological differences.

2.2 Comparison of Component Catalogs

While the emission morphology lacks obvious impact from the *uv*-range applied to the calibration, this does not prevent systematic effects that could be introduced to the source flux densities, spectral indices, and beam shapes as a result of the spatially resolved calibrator at short baselines. Thus, we need to also examine the measurements made toward the collective sources detected in an image. We use eight images in tiles T19t20 and T16t29 to create two

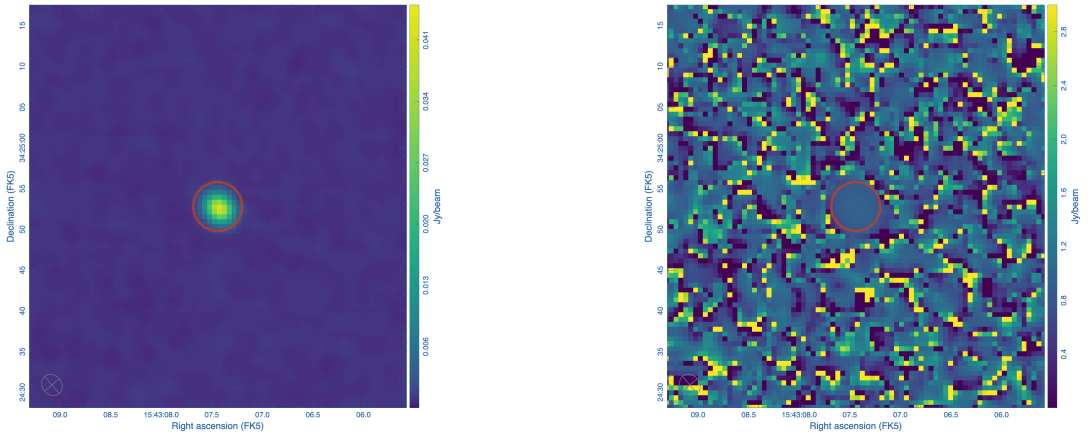

(a) (b)

Figure 5: (a) displays the point source for the image with *uv*-range applied calibration and (b) displays the same region (in red) of the uvrange image divided by the non-uvrange data.

	UV-range	**No UV-range**	**Relative Difference**
Center X (arcsec)	21:15:18.54 ± 0.000154	21:15:18.54 ± 0.000458	0.115
Center Y (arcsec)	23:49:33.74 ± 0.00568	323:49:33.74 ± 0.00499	0.196
Amplitude (Jy/beam)	0.026 ± 0.000159	0.027 ± 0.000129	3.24
Major Axis (arcsec)	2.88 ± 0.0205	3.16 ± 0.0175	7.26
Minor Axis (arcsec)	2.10 ± 0.0110	2.31 ± 0.00955	10.1
P.A. (deg)	64.23 ± 0.667	62.30 ± 0.528	1.62
Integrated flux (Jy)	0.0280 ± 0.000294	0.0292 ± 0.000240	2.28

Table 4: Comparison of component parameters for a point source in J211512+233000.

collective samples of sources in various regions of the sky.

2.2.1 VLASS 2.1: T19t20

We begin by extracting components from each image using *pyBDSF*, a component catalog generation package, which is run on the SE continuum images following the SE continuum imaging pipeline. We define a cutoff for each source in the catalog with a flux density of 1.5 mJy to determine if the source is a legitimate source. Once a flux cutoff has been determined we use TOPCAT, an interactive graphical viewer and editor for tabular data, to match catalogs created from calibrations processed with and without a *uv*-range, which are matched with a maximum separation of 2". Figure 10 displays the matched sources over the 1.5mJy cutoff for the eight images used across tile T19t20.

We then use the peak flux density divided by the total flux density to determine whether or not the source is a point source. In Figure 11 we plot histograms of peak flux density/total

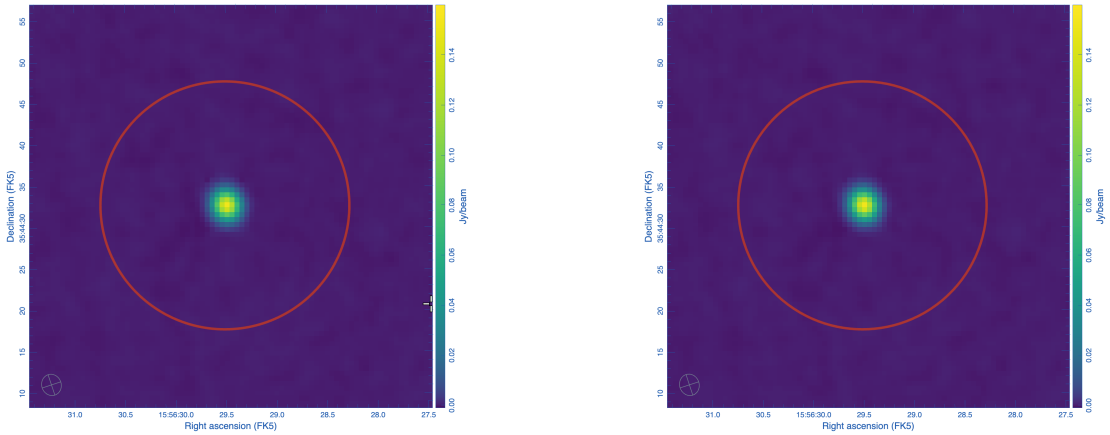

(a) (b)

Figure 6: Point source in J155758+353000 with a *uv*-range applied to the calibration in (a) and without the *uv*-range in (b). The RA and Dec of the point source is 15:56:29.51 35:44:32.7

flux density for each calibration. When peak flux density/total flux density is on the order unity, we deduce it is a point source. We allow for up to 10% variation in the peak flux density/total flux density thus using a cutoff 0.9 to 1.1 to signify a point source, which is shown in Figure 11. The intersection of *uv*-range point sources and no *uv*-range point sources created a sample of 152 data points for this tile.

Next we explore the separation between the determined point sources. Figure 12 displays a histogram of the separation distance (in arcseconds) of the point sources. Almost all sources are within 0.1 arcseconds of each other. Additionally, in Figure 13 we plot the offset in right ascension and declination, in arcseconds, between the two datasets, and again, find minimal differences is the position in which the point sources are located.

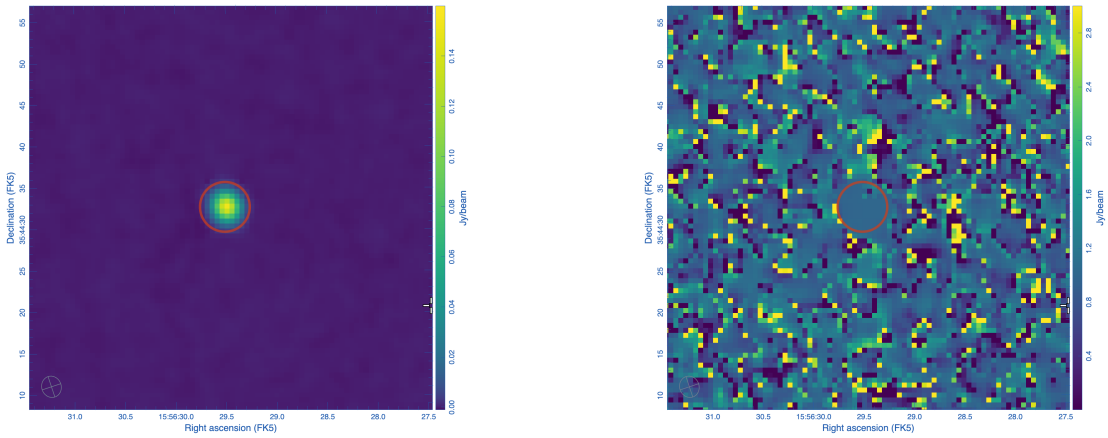

(a) (b)

Figure 7: (a) displays the point source for the image with *uv*-range applied calibration and (b) displays the same region (in red) of the uvrange image divided by the non-uvrange data.

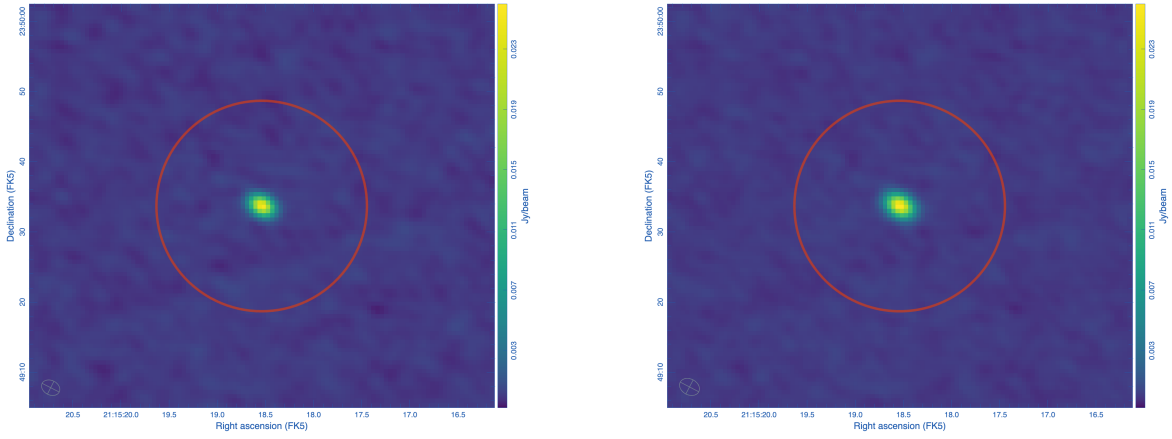

(a) (b)

Figure 8: Point source in J211512+233000 with a *uv*-range applied to the calibration in (a) and without the *uv*-range in (b). The RA and Dec of the point source is 21:15:18.54 23:49:33.7.

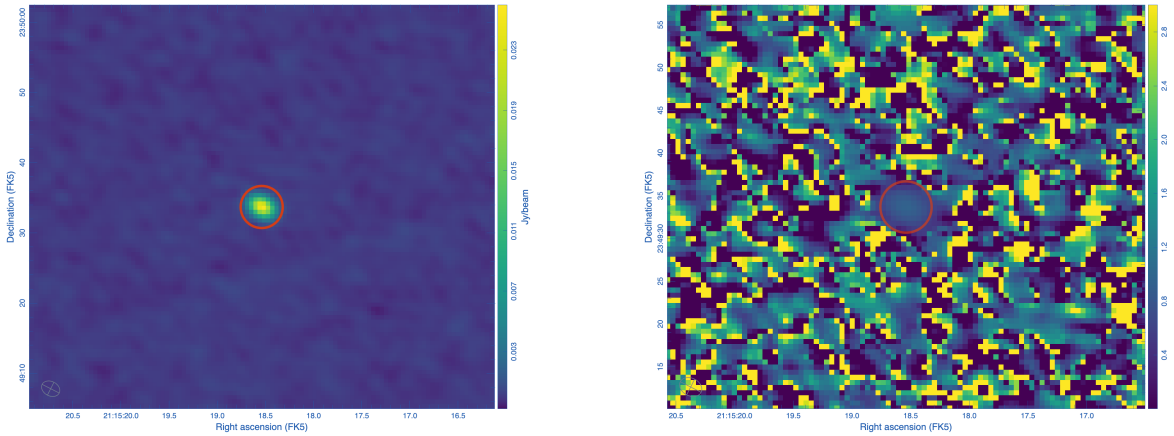

(a) (b)

Figure 9: (a) displays the point source for the image with *uv*-range applied calibration and (b) displays the same region (in red) of the uvrange image divided by the non-uvrange data.

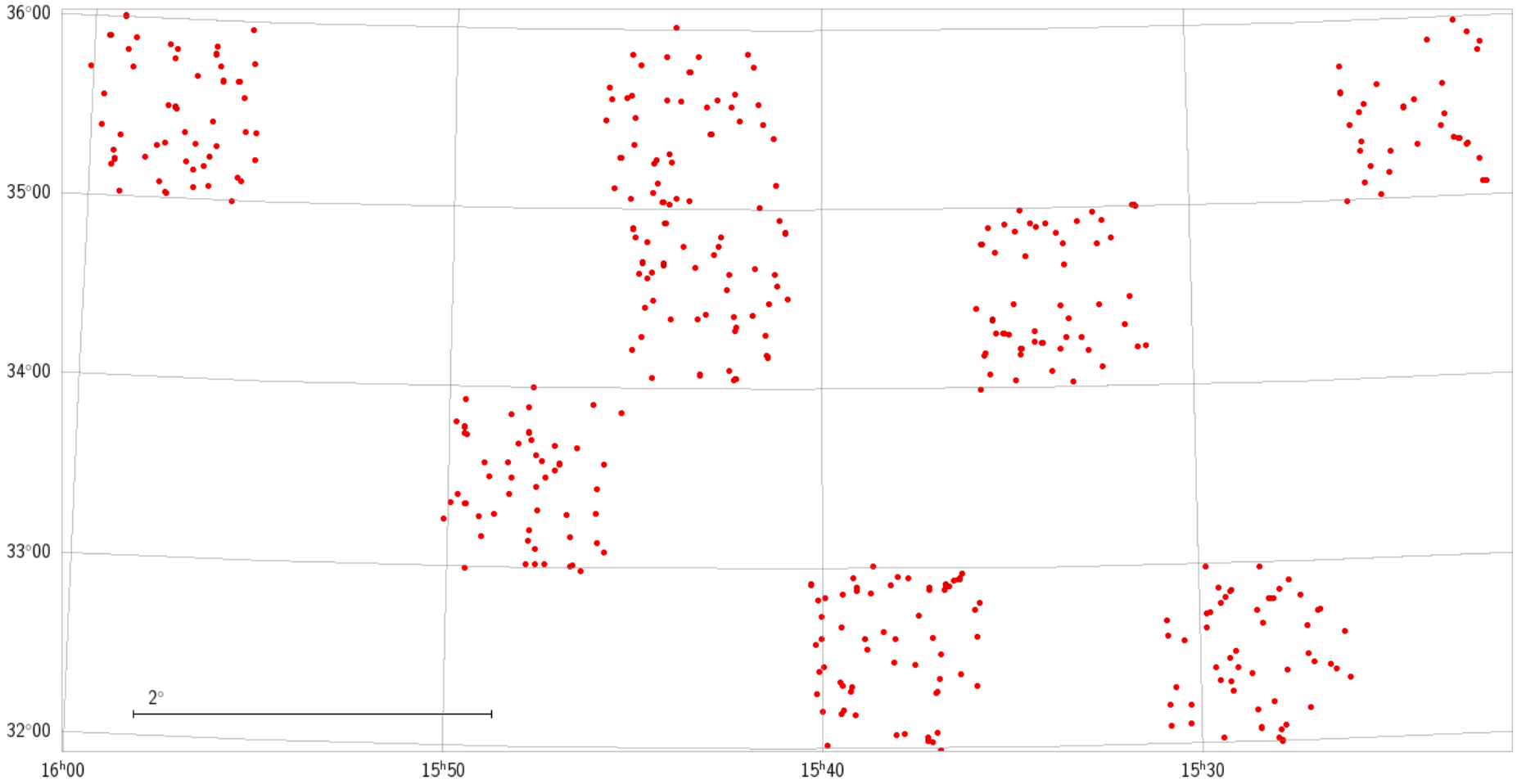

Figure 10: Map of matched point sources (within 2” separation) in T19t20 that are above a 1.5 mJy cutoff.

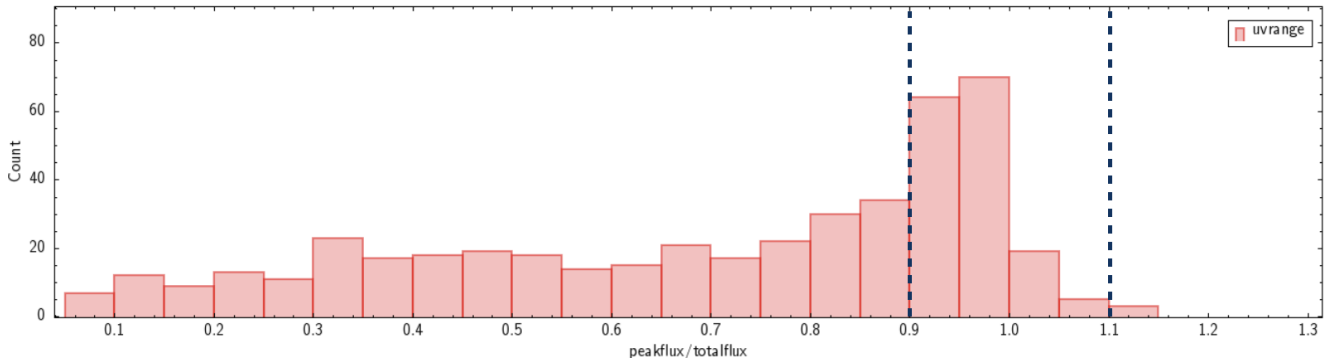

(a)

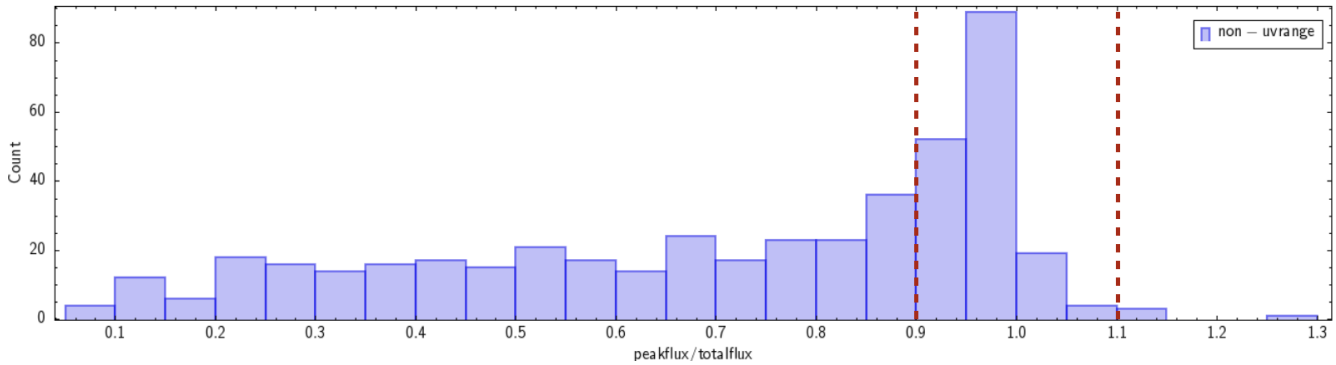

(b)

Figure 11: Histograms for T19t20 of values for peak flux density/total flux density with cutoffs indicated with dashed lines. Cutoffs range from 0.9 to 1.1, accounting for a 10% variation. (a) corresponds to data taken from the calibration with a *uv*-range applied and (b) corresponds to data take from the calibration without a *uv*-range applied.

Peak flux density for both *uv*-range calibration and without a *uv*-range calibration are compared via a scatter plot. Figure 14 displays this scatter plot on a log scale with a linear model fit to the data. We report a slope of 0.995, indicating a very small difference between peak fluxes for the 152 point sources across the tile with the uvrange having slightly higher flux densities by <1%. Similarly, in Figure 15 we plot the total flux density for the calibration processed with and without a *uv*-range applied with a linear model fit to the data. We find a slope of 0.996, indicating very little difference in the total flux density between the two calibrations.

2.2.2 VLASS 2.2: T16t29

The process for T16t29 follows the analysis for T19t20 in Section 2.2.1. We extract components from each image using *pyBDSF*, define a cutoff for each source in the catalog with a flux density of 1.5 mJy, use TOPCAT to match catalogs created from calibrations processed with and without a *uv*-range, which are matched with a maximum separation of 2". Figure

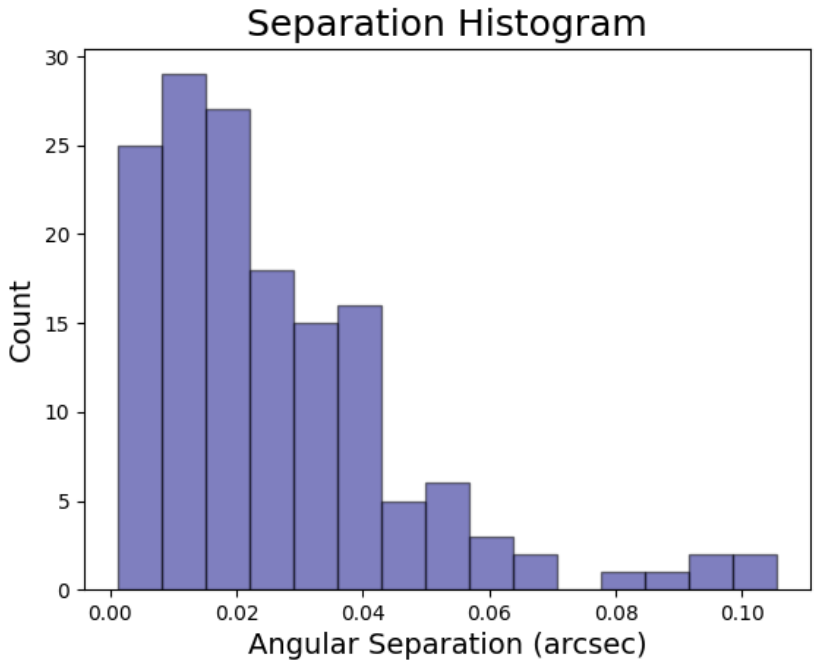

Figure 12: Histogram for T19t20 of separation for each source in units of arcseconds.

16 displays the matched sources over the 1.5 mJy cutoff for the eight images used across tile T16t29.

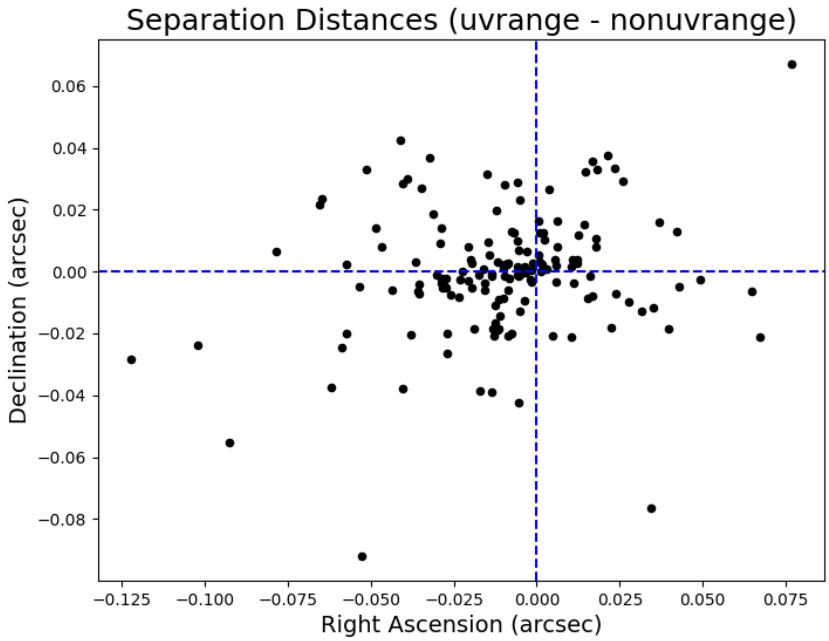

Figure 13: Scatter plot displaying the difference in right ascension and declination for each point source in tile T19t20.

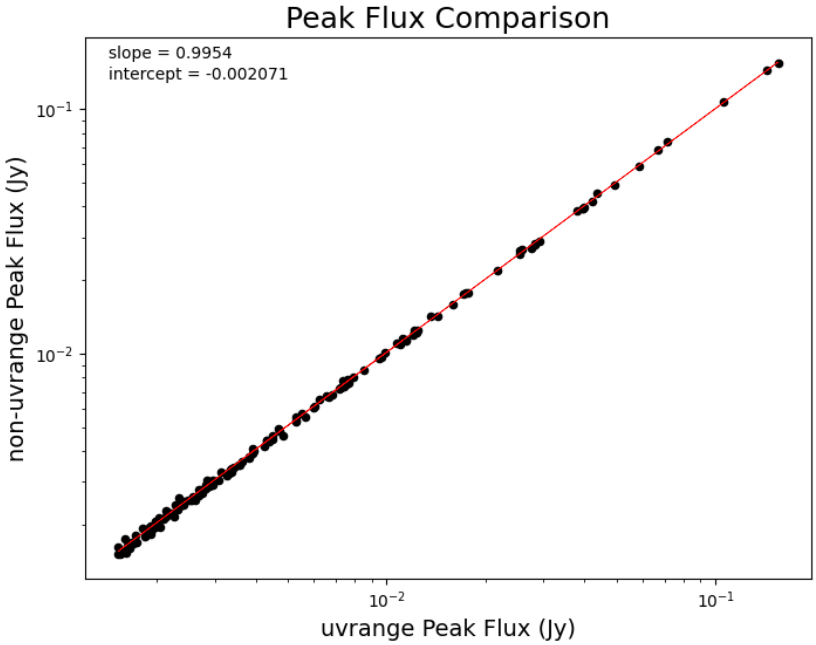

Figure 14: Scatter plot of peak flux density for *uv*-range versus no *uv*-range applied with a linear model fit to the data for T19t20.

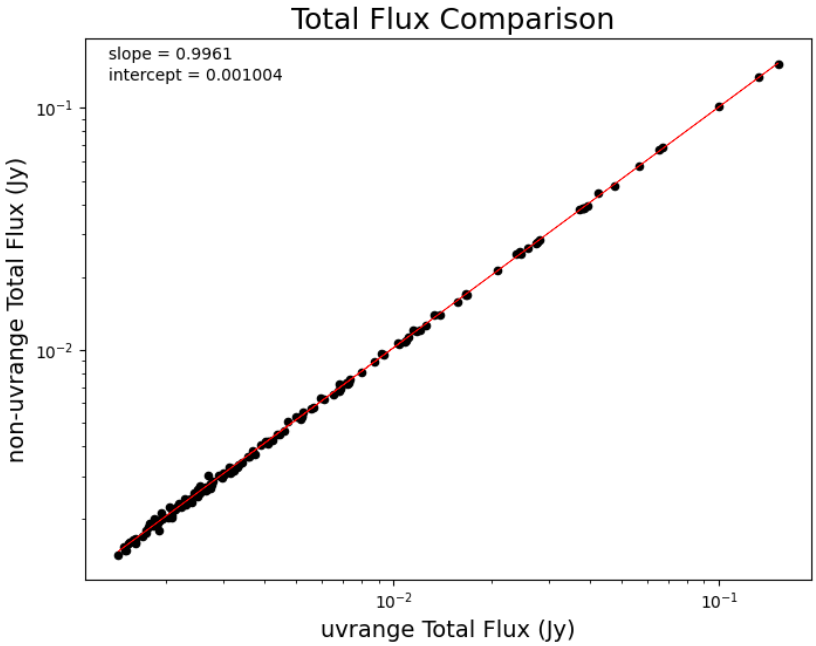

Figure 15: Scatter plot of total flux density for *uv*-range versus no *uv*-range with a linear model fit to the data for T19t20.

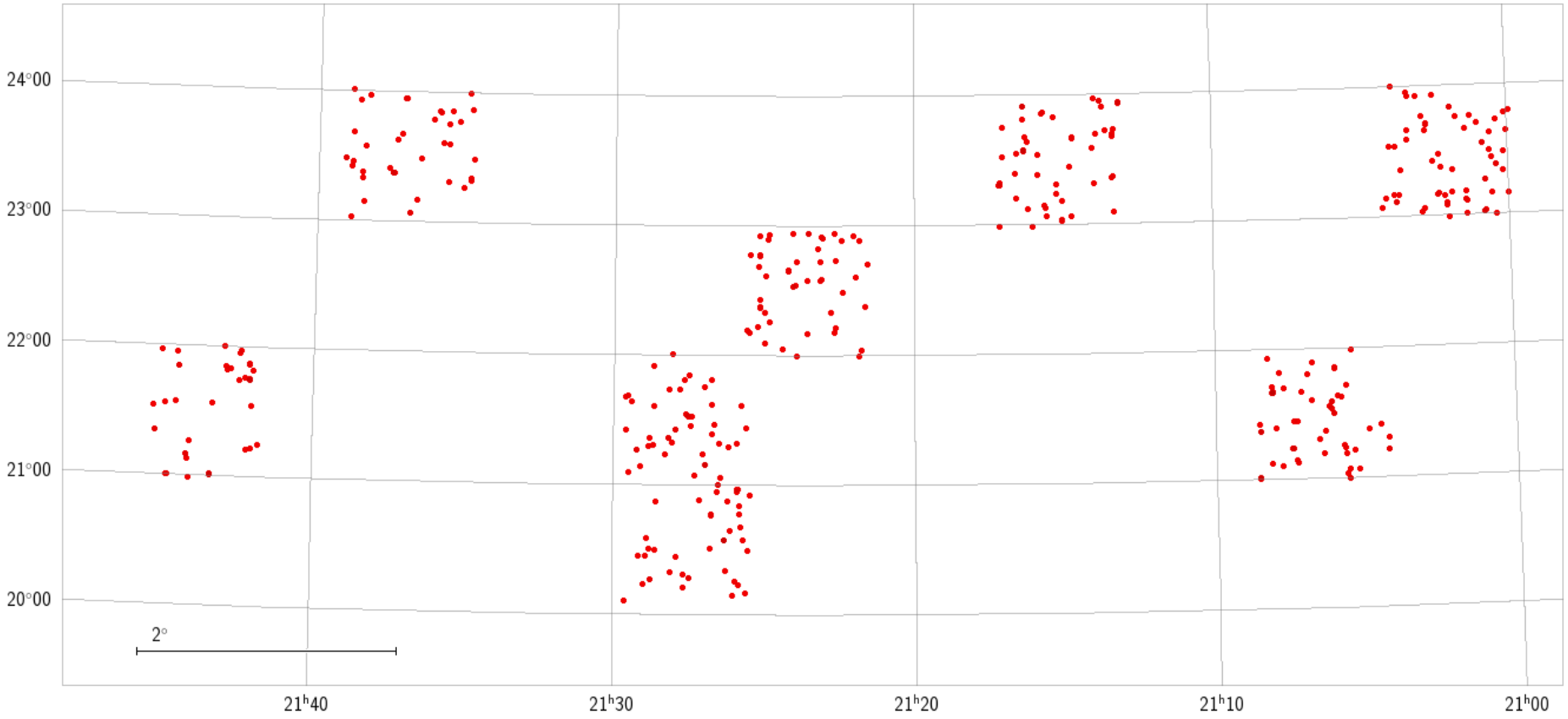

Figure 16: Map of matched point sources (within 2” separation) in T16t29 that are above a 1.5 mJy cutoff for T16t29.

Using the peak flux density divided by the total flux density, we determine whether the detected source is a point source. In Figure 17 we plot histograms of peak flux density/total flux density for calibrations with and without a *uv*-range applied. When peak flux density/total flux density is on the order unity, we deduce it is a point source. We allow for up to 10% variation in the peak flux density/total flux density thus using a cutoff 0.9 to 1.1 to signify a point source, which is shown in Figure 17. Between all eight images, we collect a total of 98 point sources for this tile.

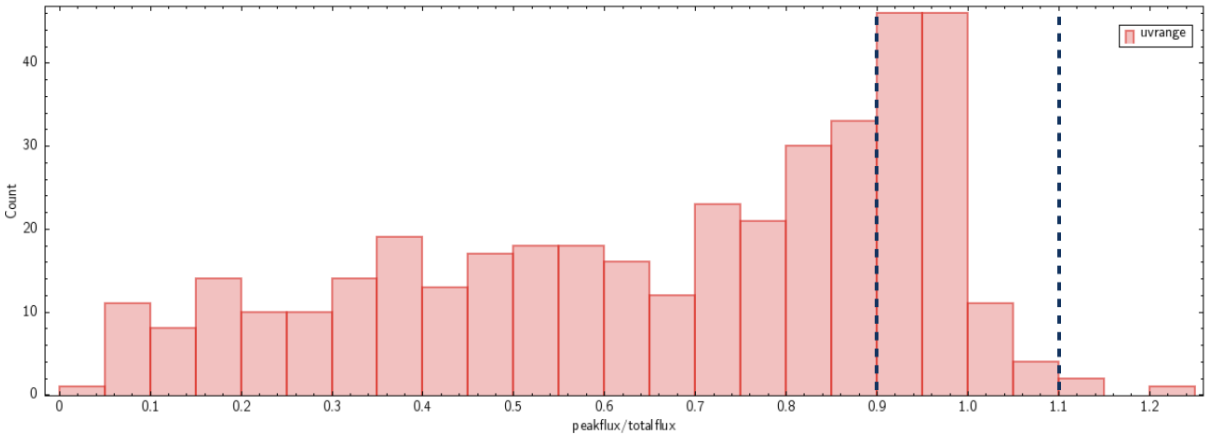

(a)

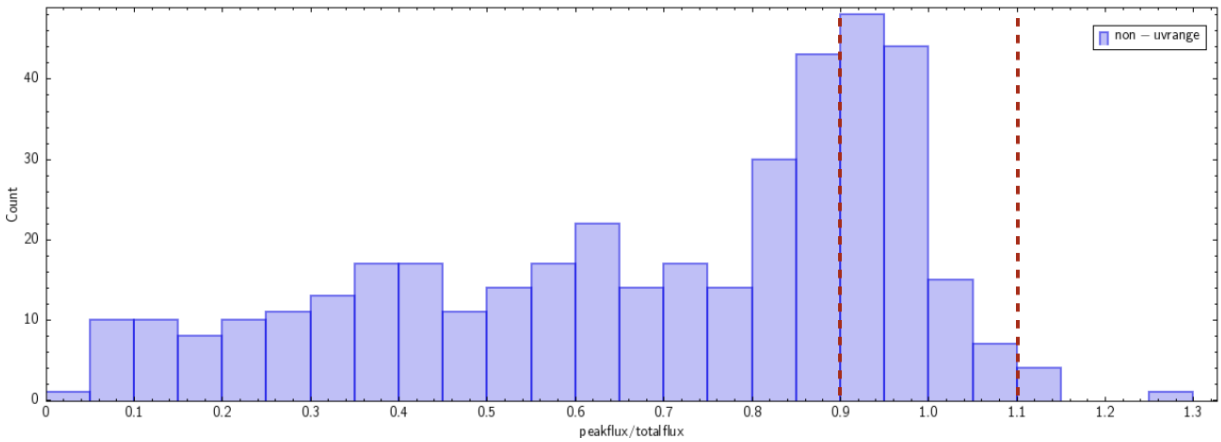

(b)

Figure 17: Histograms for T16t29 of values for peak flux density/total flux density with cutoffs indicated with dashed lines. Cutoffs range from 0.9 to 1.1, accounting for a 10% variation. (a) corresponds to data taken from the calibration with a *uv*-range applied and (b) corresponds to data take from the calibration without a *uv*-range applied.

Next we explore the separation between the determined point sources. Figure 18 displays a histogram of the separation distance (in arcseconds) of the point sources. Almost all sources are within 0.2 arcseconds of each other. Additionally, in Figure 19 we plot the offset in right ascension and declination, in arcseconds, between the two datasets, and again, find minimal

differences in the position in which the point sources are located.

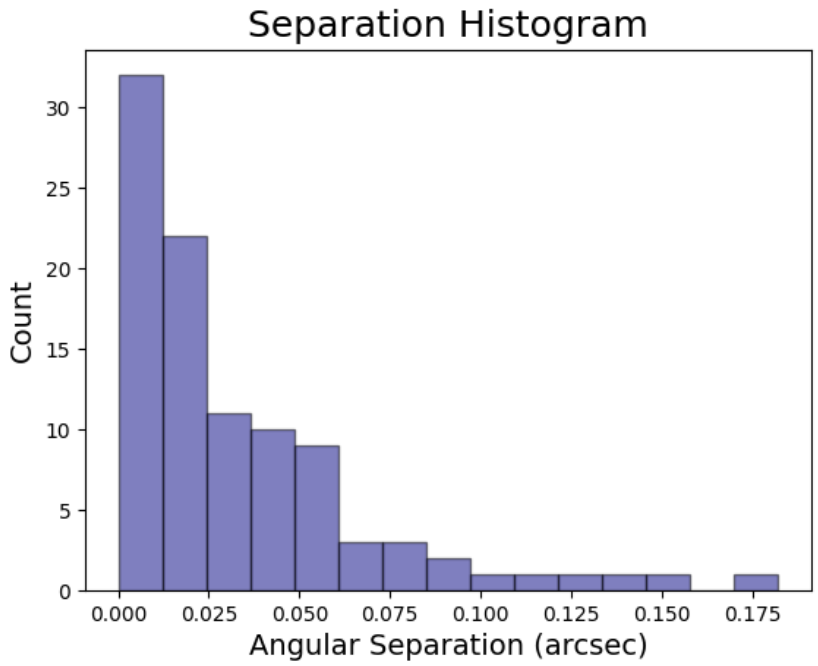

Figure 18: Histogram for T16t29 of separation for each source in units of arcseconds.

Peak flux density for both *uv*-range calibration and without a *uv*-range calibration are compared via a scatter plot. Figure 20 displays this scatter plot on a log scale with a linear model fit to the data. We report a slope of 0.994, indicating a very small difference between peak flux densities for the 98 point sources across the tile. Similarly, in Figure 21 we plot the total flux density for the calibration processed with and without a *uv*-range applied with a linear model fit to the data. We find a slope of 0.995, indicating very little difference in the total flux density between the two calibrations, with the uvrange image sources having slightly higher flux densities by <1%.

3 Conclusions and Recommendation to the VLASS Project

Overall, we aim to recommend whether or not to apply *uv*-range minimums to data where the complex gain calibrator is not a point source at all spatial scales. For the sample created, the images created from data calibrated with and without a *uv*-range show only minor differences. We have shown little to no impact on the source morphology in visual comparison between the two calibrations, and the component properties from the images also do not show significant differences in total flux density or peak intensity for point sources. Thus, the minimal quantitative differences of component properties do not indicate that

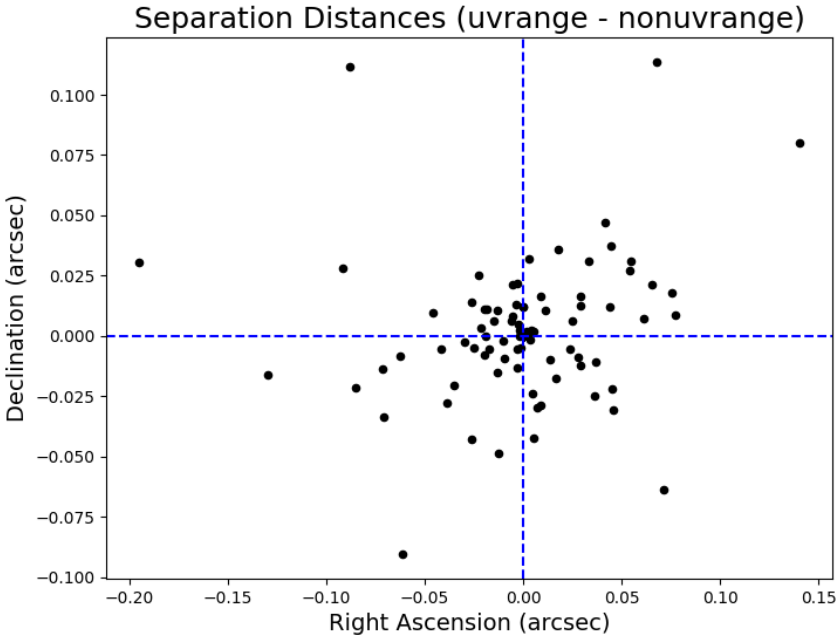

Figure 19: Scatter plot displaying the difference in right ascension and declination for each point source for T16t29.

calibration with a *uv*-range results in a considerable difference from calibration without a *uv*-range. We recommend *not* re-calibrating data to apply a *uv*-range and continue future single epoch imaging with quicklook calibrations.

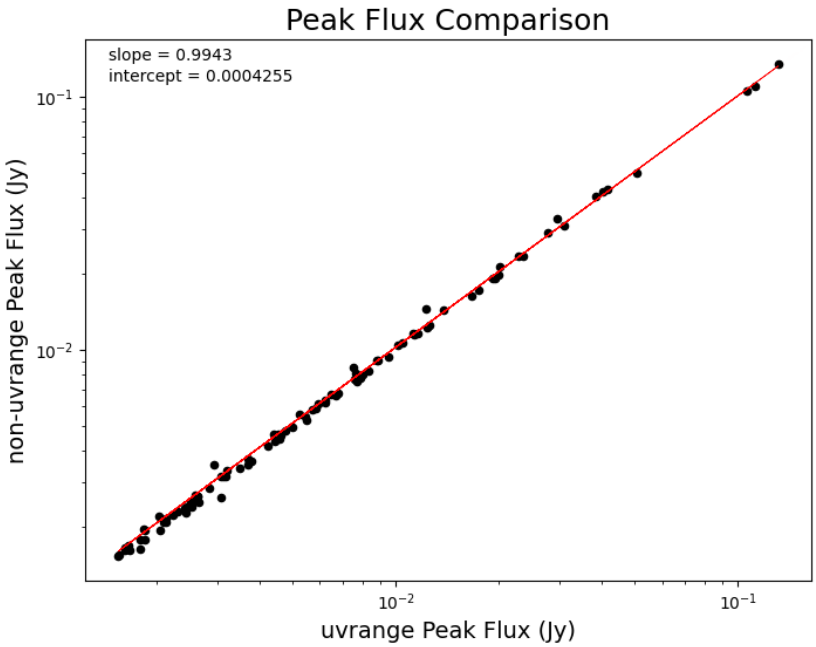

Figure 20: Scatter plot of peak flux density for *uv*-range versus no *uv*-range applied with a linear model fit to the data for T16t29.

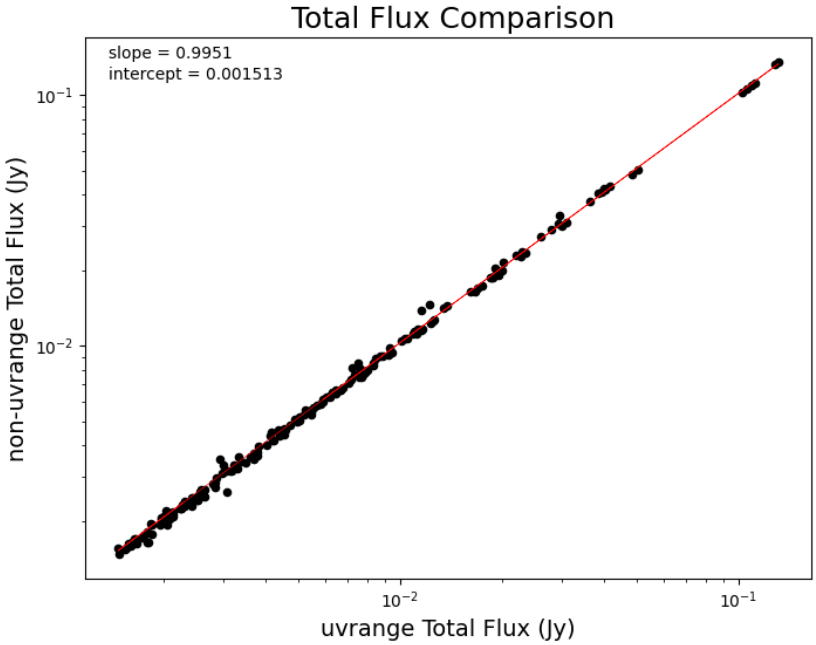

Figure 21: Scatter plot of total flux density for *uv*-range versus no *uv*-range with a linear model fit to the data for T16t29.